Published in final edited form as:

Mol Neurobiol. 2016 July ; 53(5): 3477–3493. doi:10.1007/s12035-015-9295-y.

Matrix Metalloproteinase-9 regulates neuronal circuit development and excitability

Sachiko Murase[1,2], **Crystal Lantz**[2], **Eunyoung Kim**[3], **Nitin Gupta**[4], **Richard Higgins**[2], **Mark Stopfer**[4], **Dax A. Hoffman**[3], and **Elizabeth M. Quinlan**[2]

[1]Laboratory of Molecular Biology, National Institute of Neurological Disorder and Stroke, National Institutes of Health, Bethesda, MD 20892

[2]Department of Biology and Neuroscience and Cognitive Sciences Program, University of Maryland, College Park, MD 20742

[3]Molecular Neurophysiology and Biophysics Section, Program in Developmental Neuroscience, Eunice Kennedy Shriver National Institute of Child Health and Human Development, National Institutes of Health, Bethesda, MD 20892

[4]Laboratory of Cellular and Synaptic Neurophysiology, Eunice Kennedy Shriver National Institute of Child Health and Human Development, National Institutes of Health, Bethesda, MD 20892

Abstract

In early postnatal development, naturally occurring cell death, dendritic outgrowth and synaptogenesis sculpt neuronal ensembles into functional neuronal circuits. Here we demonstrate that deletion of the extracellular proteinase MMP-9 affects each of these processes, resulting in maladapted neuronal circuitry. MMP-9 deletion increases the number of CA1 pyramidal neurons, but decreases dendritic length and complexity while dendritic spine density is unchanged. Parallel changes in neuronal morphology are observed in primary visual cortex, and persist into adulthood. Individual CA1 neurons in MMP-$9^{-/-}$ mice have enhanced input resistance and a significant increase in the frequency, but not amplitude, of miniature excitatory postsynaptic currents (mEPSCs). Additionally, deletion of MMP-9 significant increases spontaneous neuronal activity in awake MMP-$9^{-/-}$ mice and enhances response to acute challenge by the excitotoxin kainate. Thus MMP-9-dependent proteolysis regulates several aspects of circuit maturation to constrain excitability throughout life.

Keywords

extracellular matrix; cell death; dendritic morphology; spontaneous activity; kainate-induced seizure

Correspondence should be addressed to Sachiko Murase, Department of Biology and Neuroscience and Cognitive Sciences Program, University of Maryland, College Park, MD 20742. Tel: 1-301-405-7222. smurase@umd.edu.

Introduction

During neonatal development, central nervous system circuits are refined by naturally occurring cell death (Oppenheim, 1991), dendritic outgrowth and branching (Wong & Ghosh, 2002), as well as synapse formation and pruning (Harris *et al.*, 1992). Each of these processes regulated by interactions between extracellular matrix (ECM) proteins, including laminin, fibronectin and collagen (Lander *et al.*, 1985; Gary *et al.*, 2003; Rohrbough *et al.*, 2007; Murase *et al.*, 2011), and their cognate receptors, including integrins and other cell adhesion molecules (Hynes, 2002). Matrix-metalloproteinases (MMPs) are extracellular zinc-dependent endopeptidases that regulate these processes by degrading ECM proteins and/or reducing extracellular ligand concentrations (Wlodarczyk *et al.*, 2011; Huntley, 2012). The importance of MMP-9 in both developing and mature circuits, as well as the relative stability of proteolytic changes in ECM have prompted renewed interest in understanding the role of MMP-9 activity (Tsien, 2013; Stawarski *et al.*, 2014).

In the first postnatal week, hippocampal neurons go through a period of naturally occurring cell death, which eliminates as many as half of the extant neurons (Gould *et al.*, 1991; Ferrer *et al.*, 1994). Recently, we reported that the transmembrane receptor integrin β1 is required for sustained activation of the serine/threonine kinase, Akt, a critical survival signal for hippocampal neurons during this developmental stage (Murase *et al.*, 2011). MMP-9 dependent proteolytic cleavage of laminin, an extracellular matrix glycoprotein and the ligand for integrin β1, decreases induction of the Akt survival pathway and decreases neuronal survival (Murase & McKay, 2012).

Neurons in the adult hippocampus continue to express MMP-9 (Szklarczyk *et al.*, 2002), and activity-dependent transcription, local translation, and release of MMP-9 is implicated in morphological plasticity of mature circuits (Dziembowska *et al.*, 2012). For example, MMP-9 activity is required for the synapse-specific enlargement of dendritic spines associated with expression of late-phase LTP in hippocampus (Wang *et al.*, 2008). The LTP induced by application of cAMP analogue results in an MMP-9-dependent enlargement of dendritic spines and immobilization of GluA1-containing AMPARs (Szepesi *et al.*, 2014). Inhibition of MMP-9 blocks the spine enlargement and increase in spine density induced by cocaine relapse following extinction (Smith *et al.*, 2014). Furthermore, deletion or inhibition of MMP-9 impairs the expansion of receptive fields of spared inputs in both visual and somatosensory systems (Kaliszewska *et al.*, 2012; Spolidoro *et al.*, 2012). However, epileptic discharges elevate MMP-9 activity to pathogenic levels (Szklarczyk *et al.*, 2002), inducing apoptosis (Gu *et al.*, 2005), and aberrant turnover of dendritic spines (Wilczynski *et al.*, 2008). The mossy fiber sprouting and reciprocal synaptogenesis between dentate gyrus granule cells, which creates positive feedback thought to promote seizure recurrence (Rakhade & Jensen, 2009), is thought to be promoted by seizure induced increase in MMP-9 activity (Wilczynski *et al.*, 2008). Thus MMP-9 has been implicated as an effector in the genesis of epilepsy (Lukasiuk *et al.*, 2011).

Changes in dendritic volume and spine number are the hallmarks of many neurological disorders (Garey *et al.*, 1998; Pfeiffer & Huber, 2007; Knobloch & Mansuy, 2008), and, as such, MMP-9-dependent regulation of neuronal morphology and excitability represents a

potential therapeutic target for these diseases (Huntley, 2012). Indeed, genetic ablation of MMP-9 was recently shown to reverse aspects of fragile X mental retardation 1 (Fmr1) deficiency (Sidhu *et al.*, 2014). However, the role of MMP-9 in the development and maintenance of normal neuronal circuitry is not well understood. Here we address this question by examining the consequence of genetic ablation of MMP-9 on neonatal and adult neuronal morphology and circuit excitability.

Material and Methods

Subjects

MMP-$9^{-/-}$ mice (Vu *et al.*, 1998) on FVB/NJ (wild type) background were purchased from Jackson Laboratory (Bar Harbor, ME). Equal numbers of males and females were used. All procedures conformed to the guidelines of the US Department of Health and Human Services and the University of Maryland and NIH Institutional Animal Care and Use Committees.

Dissociated primary hippocampal culture

Cultures were prepared as described previously (Murase & McKay, 2006). Hippocampi from embryonic day 18 (E18) wild type or MMP-$9^{-/-}$ mouse embryos of either sex were used for astrocyte (plated at a density of 80,000 cells/ml) and neuron (density: 200,000 cells/ml) cultures. Astrocytes were cultured in Neurobasal (Invitrogen) with 5% fetal bovine serum (FBS) in 5% CO_2 at 37°C for 14 days. Medium was changed completely twice weekly. Neurons were plated on confluent astrocyte beds and cultured in Neurobasal and B27 in 5% CO_2 at 37°C. Half of the medium was changed every 2 days.

Transfection

Transfection was performed using Lipofectamine 2000 (Invitrogen). Cells were transfected with 1.6 μg/ml of pEGFPC1 vector (Clontech, Mountain View, CA) for 15 min, and the medium was replaced with NeuroBasal Medium.

Immunostaining

Cultures were fixed with 4% paraformaldehyde (PFA), permeabilized in 0.5% Triton X-100. For *in situ* staining, subjects were perfused with PBS, then 4% PFA, and fixed with 4% PFA overnight followed by 20% sucrose containing PBS for 1 day at 4 °C. Coronal slices were made either with a Leica VT100S vibrating microtome (Leica, Allendale, NJ) at a thickness of 35 μm or with a Leica CM1520 cryostat at a thickness of 18 μm. For cryostat sectioning, brains were briefly frozen in 2-methyl-butane (Sigma-Aldrich, St Louis, MO) chilled with dry ice, and embedded in OCT compound (Tissue-Tek, Torrence, CA). Samples were blocked with phosphate buffered saline (PBS) containing 5% normal goat serum (NGS, Vector Laboratories, CA). Primary and secondary antibodies were diluted with the blocking solution. Samples were incubated for 2 hr with antibodies.

Antibodies

Antibodies were used at the following dilutions: monoclonal mouse anti-MAP2 (Sigma-Aldrich), 1:1000; polyclonal rabbit anti-cleaved caspase3 (c-cas3; Cell Signaling Technology, Danvers, MA), 1: 500; monoclonal mouse anti-NeuN (BD Biosciences), 1:500; monoclonal mouse anti-vesicular glutamate transporter 1 (VGluT1) and rabbit polyclonal anti-vesicular gamma aminobutyric acid (GABA) transporter (VGAT; Synaptic Systems, Goettingen, Germany), 1:500; polyclonal c-fos (Santa Cruz Biotechnology, Santa Cruz, CA), monoclonal mouse Reca-1 (Bio-Rad, AbD Soretc, Raleigh, NC), 1:100; polyclonal rabbit anti-glial fibrillary acidic protein (GFAP; Dako, Carpinteria, CA): 1:1000; 1:500; Alexa Fluor488 (and 568)-conjugated goat anti-mouse (and rabbit) IgG (Invitrogen, Eugene, OR), 1:200.

Image quantification

Fluorescent images were acquired on a Zeiss LSM-510 confocal microscope. Maximal intensity projections of z-stacks (8 images of 0.3 μm interval) were analyzed with ImageJ. Acquisition parameters including laser intensity, gain, pinhole, scan speed and intensity thresholds and size detection thresholds were constant for all analysis within an experiment. For cell survival assessment, images were taken from 5 fields: one from the center of the coverslip, and two vertically and two horizontally 400–3000 μm from the center. To avoid potential artifacts, neuronal densities near the rim of the cover slip, which are typically higher, were not analyzed. The mean number of neurons in the 5 fields was then quantified, with each coverslip considered a separate observation. For *in situ* analysis of apoptotic neurons, consecutive coronal cryostat sections of 18 μm thickness were analyzed. Because only small numbers of neurons were c-cas3^{+}, apoptotic neurons were screened through the hippocampal slices by eye using 10x lens. Every fourth section was used for immunohistochemistry. The total number of sections from the rostral to caudal ends of the hippocampus equaled ~ 160. For VGluT1 and VGAT immunostaining analysis, coronal sections of 35 μm thickness were used. Z-stacked images from 8 sections (0.3 μm intervals) of CA1 SLM were taken with 63x lens. Brains from each genotype were stained in parallel. Mean value for each hippocampus, in which 5 images from 5 slices were analyzed, was compared. For c-fos immunostaining analysis, Z-stacked images from 8 sections (1 μm intervals) of CA1 SP were taken with 25x lens. Mean value for each hippocampus, in which 5 images from 5 slices were analyzed, was compared. All analyses were performed blind.

Stereology

To count the total number of CA1 pyramidal neurons, every 12th coronal section of 40 μm thickness (total 7 slices per hippocampus) was immunostained with NeuN. CA1 stratum pyramidale was first outlined using a 4x lens, in which 100 × 100 μm grids were randomly placed using Stereo Investigator (MBF Bioscience, Williston, VT). Non-biased counting was performed within a three-dimensional optical dissector (30 × 30 μm) at pre-determined positions by the software using a 40x lens. The optical dissector height (thickness) was 15 μm with a 2 μm top guard zone. Mean value of both hippocampi was used as the total number for each subject. Six subjects were analyzed per condition. Parameters of stereological analysis were: Mean±SEM number of dissectors counted per hippocampus,

100.3±3.9 for P14 WT; 92.2±3.8 for P14 KO; 86.3±8.4 for P120 WT; 85.2±4.6 for P120 KO; mean±SEM number of neurons counted per hippocampus, 179.3±11.2 for P14 WT; 249.7±7.8 for P14 KO; 193.5±15.3 for P120 WT; 248.3±7.6 for P120 KO; Coeffecient error (CE) Gundersen (m=1), 0.15 for P14 and P120 WT; 0.14 for P14 and P120 KO.

Golgi staining and analysis of dendritic morphology

Golgi staining was performed using FD Rapid GolgiStain Kit (FD NeuroTechnologies). The brains were immersed in solution A and B for 1 week at room temperature and transferred into solution C for 5 days at 4°C. Coronal brain slices were made with a Leica VT100S vibrating microtome at a thickness of 150 μm. Slices were mounted on gelatin-coated slides (FD NeuroTechnologies). Neurolucida software (MicroBrightField) with a Nikon Eclipse E800 bright-field microscope with 60x lens was used to trace dendrites. Traces were analyzed with Neuroexplorer software (MicroBrightField). Because the dendritic morphology of CA1 pyramidal neurons differ between dorsal lateral and ventral parts of the hippocampus (Dougherty *et al.*, 2012), only dorsal lateral hippocampus were used for analysis. In V1, layer IV was identified by the presence of stellate neurons. Pyramidal neurons (with long apical dendrite and pyramidal somata) located immediate below layer IV were used for analysis. Three to 4 animals of each genotype were used.

Spine density analysis

Oblique dendrites of GFP-expressing pyramidal neurons from culture, and Golgi-stained CA1 pyramidal neurons *in situ* were analyzed for spine density. We reasoned that the shorter dendrites of MMP-9 KO neurons would introduce bias into a Sholl analysis, and therefore we focused analysis on oblique dendrites. Oblique dendrites have also been implicated in epilepsy-induced changes in hippocampal excitability induced by epilepsy (Ang *et al.*, 2006). Fluorescent images were analyzed using ImageJ. Golgi staining was traced using Neurolucida, and analyzed in Neuroexplorer. For fluorescent images, mean value for each neuron was compared. For Golgi staining, mean value for each hippocampus, in which 5 neurons were analyzed, was compared.

NEURON models and simulations

Simulations were performed in NEURON, version 7.3 (Hines & Carnevale, 1997). Each cell was represented by a passive, multi-compartmental model. The apical and basal dendritic compartments were extracted from experimentally observed morphology, imported from Neurolucida reconstructions into NEURON using the Import3D module. In some cases the imported files were manually edited to correct formatting. Ten wild-type and 9 MMP-9 neurons were imported and used in the analysis. Somata were modeled as cylinders with diameter and length equal to 30 μm. Axons were excluded. Passive channels were distributed uniformly across all compartments with the following parameters: membrane resistance (R_m) = 10 kΩ/cm^2; axial resistance (R_a) = 150 Ω/cm; membrane capacitance (C_m) = 1 μF/cm^2. Similar values have been used in previous models of CA1 pyramidal neurons (Bianchi *et al.*, 2012; Dougherty *et al.*, 2012). We computed the input resistance of a model neuron by injecting a hyperpolarizing current pulse at the center of the soma and measuring the resulting change in the steady state membrane potential at the same location.

Slice electrophysiology

Acute hippocampal slices (250 μm thick) were prepared from mice in a cutting solution containing (in mM): 90 Sucrose, 80 NaCl, 3.5 KCl, 25 $NaHCO_3$, 1.25 NaH_2PO_4, 10 glucose, 0.5 $CaCl_2$, 4.5 $MgSO_4$ (pH, 7.2). After 30 min incubation in normal ACSF containing: 125 NaCl, 2.5 KCl, 25 $NaHCO_3$, 1.25 NaH_2PO_4, 25 glucose, 2 $CaCl_2$, 1 $MgCl_2$, bubbled with 95% O_2, 5% CO_2 at 37°C, slices were transferred to room temperature oxygenated ACSF solution. Mice aged P21-P23 and 14 to 15 week-old were used for input resistance measurements, and miniature excitatory postsynaptic current (mEPSC) measurements, respectively.

Whole cell patch-clamp recordings were performed in CA1 pyramidal neurons. For input resistance recordings, patch electrodes (4–6 MΩ) were filled with (in mM): 20 KCl, 125 K-gluconate, 10 HEPES, 4 NaCl, 0.5 EGTA, 4 MgATP, 0.3 Tris-GTP, 10 Phosphocreatin, pH 7.25–7.2 by KOH, 290 mOsm. At −60mV holding potential, hyperpolarizing current steps (−100 pA to 0 pA in 20 pA increment, 1000 ms) were delivered. The steady-state voltage responses were plotted against the amplitude of current injection and the slope of the linear fit of this relationship was determined to calculate input resistance. For mEPSCs recordings, patch electrodes (4–6 MΩ) were filled with (in mM): 100 Cs-Gluconate, 40 HEPES, 8 NaCl, 5 $MgCl_2$, 0.6 EGTA, 2 Na2ATP, 0.3 NaGTP, 15 CsCl, pH 7.25–7.2 by CsOH, 290 msm. To isolate mEPSCs cells were held at −60mV and 10 μM Gabazine, 1 μM TTX, and 50 μM D-AP5 were added to the external solution. All recordings were acquired by using a MutiClamp 700B amplifier (Axon Instruments) and analyzed by using Clampfit 10.3 (Molecular Devices, Sunnyvale, CA), Mini Analysis (Synaptosoft), and Microsoft Excel.

Electrocorticography (ECoG) Recordings

P112-P168 mice were anesthetized with ketamine (120 mg/kg) and xylazine (9 mg/kg). Four silver recording electrodes (impedance 0.2 – 0.4 kΩ) were placed on dura through small holes drilled through the skull at 1.0 mm caudal to bregma/2.0 mm lateral to the midline, and 3.00 mm lateral to the midline/0.01 mm rostral to lambda, bilaterally. A single ground electrode was implanted 0.50 mm rostral to bregma/0.50 mm lateral to the midline. Electrodes were secured to the skull with cyanoacrylate (Loctite, Rocky Hill, CT). After implantation subjects were monitored until they recovered righting reflexes. Buprenorphine (0.1 mg/kg) was administered for post-surgical analgesia. Recordings began 3 days after implantation surgery. Prior to recording subjects were habituated to the head restraint apparatus for 10 minutes, after which baseline ECoGs were recorded from all four dural-electrodes for 30 minutes (high pass filter: 0.5 Hz, low pass filter: 300 Hz). After the initial 30 minutes subjects received 10 mg/ml of kainate (i.p.; dissolved in 0.9% sodium chloride solution), and were immediately returned to the recording apparatus and resultant ECoG activity was recorded for 120 minutes.

Absolute power spectrum density (PSD, mV^2/Hz) of baseline activity was extracted from the Fast Fourier Transform (FFT) for δ (1–4 Hz), θ (4–8 Hz), α (8–12 Hz), β (12–30 Hz), γ (30–60 Hz). Seizure initiation was identified with a custom MATLAB script with Chronux extensions (Mitra & Bokil, 2008), after removal of movement artifacts, based on simultaneous occurrence of 3 criteria: an increase in theta power, an increase in gamma

power and an increase in spiking above the mean of the recording time period, each increase of ≥2 standard deviations above average. A spike was defined as the first derivative of the waveform over 3 ms such that the first derivative of each 3 ms window was between the 50th and 90th percentiles of the cumulative distribution (similar to White *et al.*, 2006 (White *et al.*, 2006)). This analysis eliminated inclusion of small changes in voltage associated with non-seizure activity, as well as large artifacts from movement or electrical noise. An FFT was performed to transform time-domain voltage data to the frequency domain, over the length of the recording with a moving window of 10 s with a 5 s overlap. Seizure termination was identified by a rapid decrease in theta power to <2 standard deviations below the average.

Single unit recordings

Electrode implantation for the recording of single units was similar to ECoG except that a 1.2 mm 16-channel platinum-iridium electrode shank (15 – 20 kΩ) constructed in house was implanted 3.00 mm lateral to the midline/0.01 mm rostral to lambda to a depth of 1 mm, to center the electrode shank on layer IV of the visual cortex. Spontaneous single unit activity from layer IV of visual cortex is reported, confirmed by the waveform (largest negative peak) of the simultaneously acquired VEP in response to full field 0.5 second 100% contrast flash. One day prior to recording subjects were habituated to the head restraint for 45 minutes. Spontaneous single unit activity was recorded in 200 X 1 second trials (300 Hz high pass and 5 kHz low pass). Recorded single units were sorted based on waveform and fixed variable principle component analysis using Open Sorter software (TDT). Spike-rate and inter-spike interval were calculated using a custom program in MATLAB.

Seizure analysis

Adult mice (P112-P168) were given a single intraperitoneal (i.p.) injection of 20 mg/kg kainate (dissolved in 0.9% sodium chloride solution). Subjects were returned to home cage following injection, and videotaped for 2 hours. The severity of seizure induced by acute kainate challenge was classified according to the Racine scale (Racine, 1972): stage 0, normal behavior; stage 1, immobility; stage 2, repetitive forelimb clonus and rearing; stage 4, continuous rearing and falling; and stage 5, generalized tonic-chronic seizure. Subjects were perfused and processed for immunohistochemistry for c-fos 2hr after acute kainate delivery.

Statistical analyses

Statistical significance between two groups was determined with a two-tailed paired Student's T-test. For multiple groups, statistical comparisons were made by one-way or repeated measures ANOVA with Tukey-Kramer corrections for multiple comparisons. K-S test was used to assess significance of differences across distributions.

Results

Suppression of neuronal death in neonatal hippocampus of MMP-9$^{-/-}$ mice

MMP-9 dependent proteolytic cleavage of laminin decreases neuronal survival (Murase & McKay, 2012). Therefore, we first examined the effect of MMP-9 deletion on the natural cell death observed early in postnatal development. Although both neurons and astrocytes

can produce MMP-9 (Szklarczyk *et al.*, 2002), it is not known if MMP-9 from both sources can regulate neuronal survival. Therefore, hippocampal neurons from MMP-9$^{-/-}$ mice (Vu *et al.*, 1998) on FVB/NJ (wild type) background were plated at low density on astrocytes from wild type or MMP-9$^{-/-}$ mice, to identify the source of the MMP-9 regulating cell death. As expected, a significant decrease in the number of neurons, identified by labeling for the microtubule-associated protein MAP2, was observed from 5–14 days *in vitro* in all four culture-conditions (DIV5-14; Fig. 1A). However, cell death was significantly attenuated in cultures in which the neurons, but not the astrocytes, were derived from MMP-9$^{-/-}$ mice.

To ask if a similar rescue from natural cell death was observed *in vivo*, we used quantitative immunohistochemical labeling for markers of apoptosis in the hippocampus of MMP-9$^{-/-}$ mice. C-cas3, which reports the cleavage and activation of caspase 3, is a final common step of several converging apoptotic signaling pathways (Riedl & Shi, 2004). C-cas3 staining revealed apoptotic neurons, identified by colocalized NeuN labeling, in the hippocampi of wild type and MMP-9$^{-/-}$ mice (Fig. 1B). However, the number of apoptotic neurons in CA1 was significantly reduced in MMP-9$^{-/-}$ mice at postnatal day 4 (P4), the peak of the period of natural cell death.

As neurogenesis in the CA1 region of the rodent hippocampus is completed by birth (Soriano *et al.*, 1986; Finlay & Darlington, 1995), suppression of postnatal apoptosis would be expected to increase the total number of surviving hippocampal neurons. Indeed, stereological analysis of total number of neurons in the CA1 stratum pyramidale (SP) region of hippocampus reveals a significant increase in MMP-9$^{-/-}$ mice compared to the wild type at P14 (743,632±75,282 for WT, 1,048,689±94,929 for KO, n=6 subjects, p=0.03, Student's T-test). The increase in the number of neurons in MMP9$^{-/-}$ CA1 is maintained into adulthood (Fig. 1C). This implicates neuron-derived MMP-9 in the promotion of natural cell death in early development, and the absence of MMP-9 enhances neuronal survival *in vitro* and *in vivo*.

Simplified dendritic morphology and higher input resistance in MMP-9$^{-/-}$ mice

Many of the MMP-9 substrates are known to regulate neurite elongation. To ask how ablation of MMP-9 impacted dendritic outgrowth, Golgi-staining was used to examine neurite morphology of CA1 pyramidal neurons in MMP-9$^{-/-}$ mice over development. This approach allowed quantification of growth, length and complexity of neuronal dendrites. Dendritic outgrowth was modest for both genotypes during the first postnatal week, but increased rapidly during the second postnatal week, coincident the end of natural cell death period (P8, Fig. 2A and B left). However, dendritic outgrowth was significantly reduced in neurons from MMP-9$^{-/-}$ mice relative to wild type, resulting in a ≥40% reduction in total dendritic length by P14 (Fig. 2A and B). Cultured neurons transfected with GFP-expressing plasmid from MMP-9$^{-/-}$ mice have significantly shorter dendrites than wild type at DIV21 (Fig. 2B, 74.14±5.22% of wild type, n=15, neurons from 5 cultures for each group, p=0.017, Student's T-test). Quantification of dendritic branching (Fig. 2A and 2B middle) and a Sholl analysis of the number of intersections on apical and basal dendrites, revealed a decrease in dendritic complexity in neurons from MMP-9$^{-/-}$ hippocampus (Fig. 2C). No changes were observed in cell body size (Fig. 2B right).

The change in length and branching patterns of neuronal dendrites from MMP-9$^{-/-}$ mice is expected to influence intrinsic neuronal properties such as input resistance. Indeed, simulated steady-state voltage responses predicted significantly higher input resistance for CA1 pyramidal neurons from MMP-9$^{-/-}$ mice relative to wild type (Fig. 3A and B). Experimental measurements confirmed significantly higher somatic input resistance in neurons from MMP-9$^{-/-}$ mice, with no difference in resting membrane potential (Fig. 3C–F). The MMP-9-dependent changes in neuronal morphology and intrinsic properties are likely to impact neuronal excitability.

Changes in synaptic structure and function in MMP-9$^{-/-}$ Mice

Changes in dendritic architecture can impact synaptic density. As the majority of the excitatory synapses in the mammalian cortex occur on dendritic spine heads, oblique dendrites of GFP-expressing pyramidal neurons from culture, and Golgi-stained CA1 pyramidal neurons *in situ* were used to ask to ask how MMP-9 affects dendritic spines during early postnatal development. We reasoned that the shorter dendrites of MMP-9$^{-/-}$ neurons would introduce bias into a Sholl analysis, and therefore we focused analysis of dendritic spine density on oblique dendrites. Oblique dendrites have also been implicated in epilepsy-induced changes in hippocampal excitability induced by epilepsy (Ang *et al.*, 2006). Immunostaining for the pre-synaptic vesicular glutamate transporter 1 (VGluT1) colocalized 100% with dendritic protrusions, suggesting that dendritic spines and filopodia were opposed to excitatory active zones. We found that spine densities (spines per 10 μm) at 17 days *in vitro* were similar in oblique dendrites of CA1 pyramidal neurons from wild type and MMP-9$^{-/-}$ mice (Fig. 4A). Similarly, Golgi staining of neurons *in situ* revealed similar spine densities at postnatal day 14 (P14) in oblique dendrites of CA1 (Fig. 4A).

We used spine head diameters and neck lengths to ask if MMP-9 impacted the morphology of individual dendritic spines. We sorted all dendritic protrusions into three categories: Thin spines (spine head diameter<0.6 μm), stubby spines (neck length<0.2 μm), and mushroom spines (spine head diameter>0.6 mm and neck length>0.2 μm). We observed no difference in the proportion of each spine type across genotypes (Fig. 4B). Similarly, the distributions of spine head diameters and spine neck lengths were similar in MMP-9$^{-/-}$ and wild type (Fig. 4C, p=0.155 for head diameter, p=0.358 for neck length, K-S test).

For a closer examination of the density and distribution of synapses, we quantified the densities of VGluT1^{+} puncta in CA1 stratum lacunosum-moleculare (SLM) from hippocampal slices. No differences were observed in the number of VGluT1^{+} puncta in adult wild type *vs.* MMP-9$^{-/-}$ mice (Fig. 5A). However, the VGluT1^{+} puncta observed in the MMP-9$^{-/-}$ hippocampus of mice were larger and brighter than wild type (Fig. 5A). To examine the density and distribution of inhibitory synapses, we quantified the puncta immunopositive for the presynaptic GABA transporter VGAT. No differences were observed in the number of VGAT^{+} puncta, or in the fluorescence intensity or area of VGAT^{+} puncta in MMP-9$^{-/-}$ mice (Fig. 5B).

A constant number of excitatory synapses in combination with an increase in total number of neurons in MMP-9$^{-/-}$ mice might lead to a homeostatic decrease in the total number of synapses targeting each pyramidal neuron. However, whole cell recordings of CA1

pyramidal neurons in hippocampal slices from revealed a significant (89%) increase in mEPSC frequencies in adult MMP-9$^{-/-}$ compared to age-matched wild type (Fig. 6A, B). mEPSC amplitudes were unchanged (Fig. 6A, C).

We used Golgi staining to further ask if the changes in neuronal morphology described in the juvenile brain persist into adulthood. At postnatal day 150, the pyramidal neurons of CA1 region of hippocampus and layer IV–V primary visual cortex (V1) of MMP-9$^{-/-}$ mice have ≥35% shorter dendrites and ≥30% fewer branches than wild type, with no differences in size of cell body (Fig. 7A, B). We observed no difference in density of astrocytes, detected by immunostaining of GFAP between wild type and MMP-9$^{-/-}$ mice at P150 (CA1: 396.3±13.7 cells/mm^2 for wild type, 383.3±7.0 cells/mm^2 for MMP-9$^{-/-}$ mice. n=4 subjects, p=0.43. V1 layer IV–V: 133.3±20.2 cells/mm^2 for wild type, 144.4±14.3 cells/mm^2 for MMP-9$^{-/-}$ mice. n=4 subjects. p=0.67). In addition, we observed no differences in blood vessel volume, assessed by immunostaining of Reca-1 (CA: 1.52±0.17% for wild type, 1.39±0.08% for MMP-9$^{-/-}$ mice. n=4, p=0.53. V1 layer IV–V: 6.39±0.49% for wild type, 5.88±0.59% for MMP-9$^{-/-}$ mice. n=4 subjects. p=0.53).

Increased spontaneous activity in MMP-9$^{-/-}$ V1

The increase in neuron number, input resistance and mEPSC frequency predicts enhanced excitability in the neuronal circuits in the MMP-9$^{-/-}$ mouse. To test this hypothesis, we performed electrophysiological recordings in awake adult mice *in vivo*. These experiments were performed in the adult mouse visual cortex, which is highly amenable to chronic recordings in awake subjects. Spontaneous single unit activity was recorded from layer IV of visual cortex, confirmed by the waveform of the simultaneously acquired VEP. Single unit recordings revealed a significant enhancement in average spontaneous firing rate and a corresponding reduction in the interspike interval of sequential action potentials in V1 of MMP-9$^{-/-}$ mice relative to the wild type (Fig. 8A and B). Electrocorticography recordings also revealed an increase in spontaneous activity in the MMP-9$^{-/-}$ mice. Power spectrum density of ECoG recordings revealed an increase in oscillatory activity in low frequencies (δ (1–4 Hz) and θ (4–8 Hz)) and a decrease in oscillatory activity at higher frequencies (γ (30–60 Hz); Fig. 8C).

Prolonged seizures following challenge with acute kainate in MMP-9$^{-/-}$ mice

To ask if a consequence of enhanced excitability could be revealed in the response to an excitotoxin known to acutely trigger epileptic discharges, we examined the response to acute delivery of the excitotoxin kainate (20 mg/kg; i.p.), known to rapidly induce seizure activity (Ben-Ari, 1985). Kainate delivery induced a significantly increase in the number of neurons expressing the immediate early gene c-fos in MMP-9$^{-/-}$ mice relative to the wild type (Fig. 9A and B), and a significant increase in intensity of c-fos immunofluorescence across the entire hippocampus (Fig. 9A and C).

We used electrocorticography recordings (ECoG) from four sites on the surface of the dura to monitor the electrophysiological response to acute kainate delivery to wild type and MMP-9$^{-/-}$ adults. Seizure initiation was identified by simultaneous detection of 3 criteria: based on simultaneous occurrence of 3 criteria: an increase in theta power, an increase in

gamma power and an increase in spiking; each i≥2 standard deviations above average. A Fast Fourier Transform (FFT) was performed to transform time-domain voltage data to the frequency domain, over the length of the recording with a moving window of 10 s with a 5 s overlap, to extract the power of theta (4–8 Hz) and gamma (30–60 Hz). ECoG recordings confirmed an enhanced response to acute kainate challenge in MMP-9$^{-/-}$ mice (Fig. 10). Seizures were observed in the ECoG of both genotypes after a single acute injection of kainate (Fig. 10A and B), with a similar time to the first seizure (Mean±SEM: 2.48±1.04 min for wild type, 3.50±1.07 min for MMP-9$^{-/-}$, p=0.508, Student's T-test, n=7 subjects for wild type, 8 subjects for MMP-9$^{-/-}$). However, the duration of individual seizures was significantly longer in MMP-9$^{-/-}$ mice >60 mins after kainate delivery, indicating enhanced kainate-induced status epilepticus (Fig. 10C, Mean±SEM: 19.04±4.17 min for wild type, 46.41±8.22 min for MMP-9$^{-/-}$, p=0.0017, Student's T-test). Behavioral analyses using Racine's score (Racine, 1972) to monitor the response to single acute injection of kainate confirmed a significant increase in the severity and duration of seizure MMP-9$^{-/-}$ mice relative to the wild type (Fig. 10D and E).

Discussion

Early in postnatal development, regulation of neuron number, elaboration of dendrites and refinement of synaptic connectivity sculpt neuronal circuitry. Here we demonstrate that deletion of the extracellular proteinase MMP-9 affects each of these processes, resulting in maladapted neuronal circuitry with enhanced excitability. MMP-9 deletion suppresses naturally occurring cell death and decreases dendritic length and complexity. Accordingly, deletion of MMP-9 increases spontaneous neuronal activity in awake MMP-9$^{-/-}$ mice and enhances the response to acute challenge by the excitotoxin kainate. This demonstrates a previously undocumented role for MMP-9-dependent proteolysis: the regulation of several aspects of circuit maturation to constrain excitability throughout life.

Regulation of neuronal number by MMP-9

In the developing nervous system, neurons are produced in excess and subsequently eliminated during a period of naturally occurring cell death. MMP-9 expression is highest during the period of cell death (first postnatal week) and declines thereafter (Murase & McKay, 2012; Aujla & Huntley, 2014). Critical survival signals for hippocampal neurons during early neonatal development include the cell adhesion molecule integrin β1, which is required for sustained activation of the serine/threonine kinase, Akt (Murase *et al.*, 2011). MMP-9-dependent cleavage of laminin, the ligand for integrin β1, reduces the survival of hippocampal neurons (Murase & McKay, 2012), while ablation of neuronal MMP-9 significantly enhances hippocampal neuron survival *in vivo*. Although astrocytes can support neuronal survival (Nagai *et al.*, 2007; Dmytriyeva *et al.*, 2012), our results demonstrate that the loss of neuronal, but not astrocytic MMP-9 spares neurons from cell death *in vitro.* This implicates neuron-derived MMP-9 in the promotion of natural cell death in early development.

Regulation of dendritic morphology by MMP-9

After the period of natural cell death in postnatal hippocampus, dendritic outgrowth increases rapidly. In the absence of MMP-9, levels of the ECM protein laminin accumulate early in development, which may prematurely stabilize the ECM (Murase & McKay, 2012). Therefore, the significant reduction in dendritic length and complexity observed in MMP-$9^{-/-}$ mice may be the direct result of enhanced stability of ECM, which would increase physical constraints to neuronal process outgrowth. Accordingly, in dissociated cultures, where space between neurons is less restricted, there is asmaller difference in dendritic outgrowth between the wild type and MMP-$9^{-/-}$ neurons. Neuronal process outgrowth may also be indirectly impacted by MMP-9-dependent changes in vascularization or glial density. Indeed, angiogenesis requires remodeling of ECM (Heissig *et al.*, 2003), and is delayed in postnatal MMP-$9^{-/-}$ mice (Vu *et al.*, 1998). Astrogliogenesis could be promoted by enhanced ECM stability MMP-$9^{-/-}$ mice (Pan *et al.*, 2014; Vargova & Sykova, 2014). However, no differences in blood vessel volume or astrocyte density were observed in adult MMP-$9^{-/-}$ mice. Alternatively, the decreased dendritic length and complexity may be result from a homeostatic compensation to maintain a constant number of total synapses in the hippocampus. In addition, contact inhibition would play a larger role in reducing process outgrowth in hippocampus with increased total neuron numbers. Finally, the absence of MMP-9-depdnent conversion of pro-BDNF (Mizoguchi *et al.*, 2011), which inhibits neurite outgrowth (Koshimizu *et al.*, 2009), to BDNF, which promotes dendritic growth (Baj *et al.*, 2011), are also likely to play a role.

Regulation of excitatory synapse structure and function by MMP-9

Chronic high doses of MMP-9 applied to cultured hippocampal neurons induce a significant increase in elongation of spines, and an increase in the complement of thin filopodia-like spines (Bilousova *et al.*, 2009; Michaluk *et al.*, 2011). Importantly the thin immature spines that are a hallmark of fragile X mental retardation are reversed to normal spine head volumes following genetic deletion of MMP-9 (Sidhu *et al.*, 2014). In contrast, a single acute dose of MMP-9 applied to hippocampal slices produces an increase in spine head volume that occludes the spine head enlargement and LTP induced by theta burst stimulation (Wang *et al.*, 2008). The varied response to MMP-9 delivery presumably reflects differences in the density and maturation of the extracellular matrix *in vitro vs. in situ. In vivo*, LTP-inducing stimuli and appetitive learning paradigms increase MMP-9 gelatinolytic activity at excitatory synapses and/or dendritic spines, and the LTP-induced spine head enlargement is blocked by MMP inhibition(Wang *et al.*, 2008; Knapska *et al.*, 2013; Szepesi *et al.*, 2014). However, in CA1 pyramidal neurons *in situ* at P14, when neurite maturation is complete, the absence of MMP-9 results in no net change in the proportion of thin *vs.* mushroom spines nor the morphology of individual dendritic spines.

We observed that immunostaining for an excitatory presynaptic protein, VGluT1 in MMP-$9^{-/-}$ CA1 SLM showed larger puncta with higher intensity, whereas that for an inhibitory presynaptic protein, VGAT showed no change. The increase in the size and intensity of $VGluT1^{+}$ puncta in the absence of a change in the number of $VGluT1^{+}$ puncta in MMP-$9^{-/-}$ mice suggests changes in presynaptic terminal size and/or neurotransmitter reuptake capabilities. An increase in presynaptic terminal size has been associated with an

increase in the probability of neurotransmitter release (Murthy *et al.*, 2001; Thiagarajan *et al.*, 2005). The increase in mEPSC frequency in the absence of a change in marker for excitatory synapses (spine density and VGluT1 immunoreactivity) is consistent with an increase in the probability of neurotransmitter release at individual synapses, although we did not measure this directly. As spine density is normal but dendritic lengths are reduced, the increase in mEPSC frequency may compensate for the reduction in the number of synapses per neuron. Alternatively, the increase in mEPSC frequency may be a consequence of the reduction in dendritic lengths, allowing more dendrites to be spared during the slice preparation procedure. MMP-9 can also directly regulate neurotransmitter release through proteolysis of critical effectors (Mohrmann *et al.*, 2008; Varley *et al.*, 2011). For example, MMP-9-dependent proteolysis of neuroligin 1 (NLG1), a postsynaptic adhesion molecule at glutamatergic synapses, destabilizes presynaptic neurexin-1β and reduces mEPSC frequency (Peixoto *et al.*, 2012). Nonetheless, an increased mEPSC frequency is also expected in neurons with reduced dendritic arbors, as we see following MMP-9 ablation, in which fewer electrotonically distant events are filtered down to noise.

Regulation of excitability by MMP-9$^{-/-}$

The increase in neuron number, input resistance and mEPSC frequency predicted the enhanced excitability in the neuronal circuits we observed in the MMP-9$^{-/-}$ mouse. Indeed, neurons in the MMP-9$^{-/-}$ mouse have increased spontaneous activity, revealed both in the increase in spontaneous neuronal firing rate and increase in the power of oscillations at both delta and theta frequencies.

Enhanced excitability in MMP-9$^{-/-}$ cortex was further confirmed by enhanced response to acute challenge with the excitoxin kainate. However, previous work demonstrated that sensitivity to PTZ-kindling was decreased in MMP-9$^{-/-}$ mice, and increased in rats overexpressing MMP-9 (Wilczynski *et al.*, 2008). Indeed, inhibition of MMP-9 delays the onset and severity of PTZ-induced epilepsy in mice (Yeghiazaryan *et al.*, 2014). At first glance, our work appears to conflict with these findings. However, PTZ-induced kindling requires multiple (≥10) injections over a relatively short time span (<30 days) to reach the seizure severity observed following a single challenge with kainate. The slow emergence of status epilepticus in PTZ-kindling suggests that incremental strengthening of circuit elements (most notably in amygdala and hippocampus) mediates the effect. As many forms of activity-dependent synaptic strengthening are dependent on MMP-9 activity, the absence of MMP-9 would reduce the ability of the circuitry to adapt to repeated PTZ exposures, thereby slowing the emergence of kindling-induced status epilepticus. In addition, PTZ-induced kindling is dependent in part on MMP-9 dependent proteolysis of pro-BDNF (Mizoguchi *et al.*, 2011), which promotes process outgrowth and recurrent synaptogenesis, which in turn contributes to the slowly emerging status epilepticus. Thus, there are two dissociable consequences of effects of ablation of MMP-9, increased neuronal excitability and decreased synaptic plasticity, which are reflected in the enhanced response to acute single delivery of kainate, and reduced PTZ-induced kindling, respectively.

Considerable evidence demonstrates that MMP-9 activity is enhanced by seizure (Szklarczyk *et al.*, 2002; Hoehna *et al.*, 2012; Konopka *et al.*, 2013). MMP-9 has also been

implicated in neuronal death caused by seizure (Jourquin *et al.*, 2003). Interestingly, seizure-induced neuronal death is mediated by the MMP-9-dependent disruption of integrin β1-PI3K/Akt signaling (Kim *et al.*, 2009), the same survival pathway that is disrupted by MMP-9 early in neonatal natural cell death, which coincides with high MMP-9 expression levels (Murase *et al.*, 2011).

Implications

The effects of global gene knockout can be masked by the compensatory expression of functionally related genes (Thyagarajan *et al.*, 2003). However, the enhanced excitability we observed in the MMP-$9^{-/-}$ mouse indicates that the nervous system does not fully compensate for the loss of MMP-9. This is somewhat surprising, given the importance of the control of circuit excitability both for optimizing information storage and preventing pathological excitation. Although the activity-dependent release of MMP-9 is implicated in morphological plasticity of mature circuits (Dziembowska *et al.*, 2012), we propose that events occurring early in postnatal development strongly impact the phenotype of MMP-$9^{-/-}$ mouse brain throughout life. Neurons with shorter dendrites and fewer branches, similar to what we observe in MMP-$9^{-/-}$ mice, are observed in several developmental neurological disorders including Rett syndrome, fragile X mental retardation, schizophrenia and autism (Braun & Segal, 2000; Shen *et al.*, 2008; Fujita *et al.*, 2010; Janusz *et al.*, 2013; Cheng *et al.*, 2014; Della Sala & Pizzorusso, 2014). Intriguingly, these disorders are also characterized by enhanced neuronal excitability and increased frequency of epilepsy (Canitano, 2007; Guerrini & Parrini, 2012; Kidd *et al.*, 2014; Najjar & Pearlman, 2015).

Acknowledgments

This work was supported by the Intramural Research Program of the NIH, NICHD and NINDS, and R01EY016431 to EMQ.

References

Ang CW, Carlson GC, Coulter DA. Massive and specific dysregulation of direct cortical input to the hippocampus in temporal lobe epilepsy. J Neurosci. 2006; 26:11850–11856. [PubMed: 17108158]

Aujla PK, Huntley GW. Early postnatal expression and localization of matrix metalloproteinases-2 and -9 during establishment of rat hippocampal synaptic circuitry. J Comp Neurol. 2014; 522:1249–1263. [PubMed: 24114974]

Baj G, Leone E, Chao MV, Tongiorgi E. Spatial segregation of BDNF transcripts enables BDNF to differentially shape distinct dendritic compartments. Proc Natl Acad Sci U S A. 2011; 108:16813–16818. [PubMed: 21933955]

Ben-Ari Y. Limbic seizure and brain damage produced by kainic acid: mechanisms and relevance to human temporal lobe epilepsy. Neuroscience. 1985; 14:375–403. [PubMed: 2859548]

Bianchi D, Marasco A, Limongiello A, Marchetti C, Marie H, Tirozzi B, Migliore M. On the mechanisms underlying the depolarization block in the spiking dynamics of CA1 pyramidal neurons. Journal of computational neuroscience. 2012; 33:207–225. [PubMed: 22310969]

Bilousova TV, Dansie L, Ngo M, Aye J, Charles JR, Ethell DW, Ethell IM. Minocycline promotes dendritic spine maturation and improves behavioural performance in the fragile X mouse model. Journal of medical genetics. 2009; 46:94–102. [PubMed: 18835858]

Braun K, Segal M. FMRP involvement in formation of synapses among cultured hippocampal neurons. Cereb Cortex. 2000; 10:1045–1052. [PubMed: 11007555]

Canitano R. Epilepsy in autism spectrum disorders. European child & adolescent psychiatry. 2007; 16:61–66. [PubMed: 16932856]

Cheng TL, Wang Z, Liao Q, Zhu Y, Zhou WH, Xu W, Qiu Z. MeCP2 suppresses nuclear microRNA processing and dendritic growth by regulating the DGCR8/Drosha complex. Developmental cell. 2014; 28:547–560. [PubMed: 24636259]

Della Sala G, Pizzorusso T. Synaptic plasticity and signaling in Rett syndrome. Developmental neurobiology. 2014; 74:178–196. [PubMed: 23908158]

Dmytriyeva O, Pankratova S, Owczarek S, Sonn K, Soroka V, Ridley CM, Marsolais A, Lopez-Hoyos M, Ambartsumian N, Lukanidin E, Bock E, Berezin V, Kiryushko D. The metastasis-promoting S100A4 protein confers neuroprotection in brain injury. Nature communications. 2012; 3:1197.

Dougherty KA, Islam T, Johnston D. Intrinsic excitability of CA1 pyramidal neurones from the rat dorsal and ventral hippocampus. J Physiol. 2012; 590:5707–5722. [PubMed: 22988138]

Dziembowska M, Milek J, Janusz A, Rejmak E, Romanowska E, Gorkiewicz T, Tiron A, Bramham CR, Kaczmarek L. Activity-dependent local translation of matrix metalloproteinase-9. J Neurosci. 2012; 32:14538–14547. [PubMed: 23077039]

Ferrer I, Tortosa A, Blanco R, Martin F, Serrano T, Planas A, Macaya A. Naturally occurring cell death in the developing cerebral cortex of the rat. Evidence of apoptosis-associated internucleosomal DNA fragmentation. Neurosci Lett. 1994; 182:77–79. [PubMed: 7891894]

Finlay BL, Darlington RB. Linked regularities in the development and evolution of mammalian brains. Science. 1995; 268:1578–1584. [PubMed: 7777856]

Fujita E, Dai H, Tanabe Y, Zhiling Y, Yamagata T, Miyakawa T, Tanokura M, Momoi MY, Momoi T. Autism spectrum disorder is related to endoplasmic reticulum stress induced by mutations in the synaptic cell adhesion molecule, CADM1. Cell death & disease. 2010; 1:e47. [PubMed: 21364653]

Garey LJ, Ong WY, Patel TS, Kanani M, Davis A, Mortimer AM, Barnes TR, Hirsch SR. Reduced dendritic spine density on cerebral cortical pyramidal neurons in schizophrenia. J Neurol Neurosurg Psychiatry. 1998; 65:446–453. [PubMed: 9771764]

Gary DS, Milhavet O, Camandola S, Mattson MP. Essential role for integrin linked kinase in Akt–mediated integrin survival signaling in hippocampal neurons. J Neurochem. 2003; 84:878–890. [PubMed: 12562530]

Gould E, Woolley CS, McEwen BS. Naturally occurring cell death in the developing dentate gyrus of the rat. J Comp Neurol. 1991; 304:408–418. [PubMed: 2022756]

Gu Z, Cui J, Brown S, Fridman R, Mobashery S, Strongin AY, Lipton SA. A highly specific inhibitor of matrix metalloproteinase-9 rescues laminin from proteolysis and neurons from apoptosis in transient focal cerebral ischemia. J Neurosci. 2005; 25:6401–6408. [PubMed: 16000631]

Guerrini R, Parrini E. Epilepsy in Rett syndrome, and CDKL5- and FOXG1- gene-related encephalopathies. Epilepsia. 2012; 53:2067–2078. [PubMed: 22998673]

Harris KM, Jensen FE, Tsao B. Three-dimensional structure of dendritic spines and synapses in rat hippocampus (CA1) at postnatal day 15 and adult ages: implications for the maturation of synaptic physiology and long-term potentiation. J Neurosci. 1992; 12:2685–2705. [PubMed: 1613552]

Heissig B, Hattori K, Friedrich M, Rafii S, Werb Z. Angiogenesis: vascular remodeling of the extracellular matrix involves metalloproteinases. Current opinion in hematology. 2003; 10:136–141. [PubMed: 12579040]

Hines ML, Carnevale NT. The NEURON simulation environment. Neural computation. 1997; 9:1179–1209. [PubMed: 9248061]

Hoehna Y, Uckermann O, Luksch H, Stefovska V, Marzahn J, Theil M, Gorkiewicz T, Gawlak M, Wilczynski GM, Kaczmarek L, Ikonomidou C. Matrix metalloproteinase 9 regulates cell death following pilocarpine-induced seizures in the developing brain. Neurobiology of disease. 2012; 48:339–347. [PubMed: 22782080]

Huntley GW. Synaptic circuit remodelling by matrix metalloproteinases in health and disease. Nat Rev Neurosci. 2012; 13:743–757. [PubMed: 23047773]

Hynes RO. Integrins: bidirectional, allosteric signaling machines. Cell. 2002; 110:673–687. [PubMed: 12297042]

Janusz A, Milek J, Perycz M, Pacini L, Bagni C, Kaczmarek L, Dziembowska M. The Fragile X mental retardation protein regulates matrix metalloproteinase 9 mRNA at synapses. J Neurosci. 2013; 33:18234–18241. [PubMed: 24227732]

Jourquin J, Tremblay E, Decanis N, Charton G, Hanessian S, Chollet AM, Le Diguardher T, Khrestchatisky M, Rivera S. Neuronal activity-dependent increase of net matrix metalloproteinase activity is associated with MMP-9 neurotoxicity after kainate. Eur J Neurosci. 2003; 18:1507–1517. [PubMed: 14511330]

Kaliszewska A, Bijata M, Kaczmarek L, Kossut M. Experience-dependent plasticity of the barrel cortex in mice observed with 2-DG brain mapping and c-Fos: effects of MMP-9 KO. Cereb Cortex. 2012; 22:2160–2170. [PubMed: 22021911]

Kidd SA, Lachiewicz A, Barbouth D, Blitz RK, Delahunty C, McBrien D, Visootsak J, Berry-Kravis E. Fragile X syndrome: a review of associated medical problems. Pediatrics. 2014; 134:995–1005. [PubMed: 25287458]

Kim GW, Kim HJ, Cho KJ, Kim HW, Cho YJ, Lee BI. The role of MMP-9 in integrin-mediated hippocampal cell death after pilocarpine-induced status epilepticus. Neurobiology of disease. 2009; 36:169–180. [PubMed: 19631748]

Knapska E, Lioudyno V, Kiryk A, Mikosz M, Gorkiewicz T, Michaluk P, Gawlak M, Chaturvedi M, Mochol G, Balcerzyk M, Wojcik DK, Wilczynski GM, Kaczmarek L. Reward learning requires activity of matrix metalloproteinase-9 in the central amygdala. J Neurosci. 2013; 33:14591–14600. [PubMed: 24005309]

Knobloch M, Mansuy IM. Dendritic spine loss and synaptic alterations in Alzheimer's disease. Molecular neurobiology. 2008; 37:73–82. [PubMed: 18438727]

Konopka A, Grajkowska W, Ziemianska K, Roszkowski M, Daszkiewicz P, Rysz A, Marchel A, Koperski L, Wilczynski GM, Dzwonek J. Matrix metalloproteinase-9 (MMP-9) in human intractable epilepsy caused by focal cortical dysplasia. Epilepsy research. 2013; 104:45–58. [PubMed: 23182966]

Koshimizu H, Kiyosue K, Hara T, Hazama S, Suzuki S, Uegaki K, Nagappan G, Zaitsev E, Hirokawa T, Tatsu Y, Ogura A, Lu B, Kojima M. Multiple functions of precursor BDNF to CNS neurons: negative regulation of neurite growth, spine formation and cell survival. Molecular brain. 2009; 2:27. [PubMed: 19674479]

Lander AD, Fujii DK, Reichardt LF. Laminin is associated with the "neurite outgrowth-promoting factors" found in conditioned media. Proc Natl Acad Sci U S A. 1985; 82:2183–2187. [PubMed: 3856891]

Lukasiuk K, Wilczynski GM, Kaczmarek L. Extracellular proteases in epilepsy. Epilepsy research. 2011; 96:191–206. [PubMed: 21893397]

Michaluk P, Wawrzyniak M, Alot P, Szczot M, Wyrembek P, Mercik K, Medvedev N, Wilczek E, De Roo M, Zuschratter W, Muller D, Wilczynski GM, Mozrzymas JW, Stewart MG, Kaczmarek L, Wlodarczyk J. Influence of matrix metalloproteinase MMP-9 on dendritic spine morphology. J Cell Sci. 2011; 124:3369–3380. [PubMed: 21896646]

Mitra, P.; Bokil, H. Observed brain dynamics. Oxford University Press; Oxford ; New York: 2008.

Mizoguchi H, Nakade J, Tachibana M, Ibi D, Someya E, Koike H, Kamei H, Nabeshima T, Itohara S, Takuma K, Sawada M, Sato J, Yamada K. Matrix metalloproteinase-9 contributes to kindled seizure development in pentylenetetrazole-treated mice by converting pro-BDNF to mature BDNF in the hippocampus. J Neurosci. 2011; 31:12963–12971. [PubMed: 21900575]

Mohrmann R, Matthies HJ, Woodruff E 3rd, Broadie K. Stoned B mediates sorting of integral synaptic vesicle proteins. Neuroscience. 2008; 153:1048–1063. [PubMed: 18436388]

Murase S, McKay RD. A specific survival response in dopamine neurons at most risk in Parkinson's disease. J Neurosci. 2006; 26:9750–9760. [PubMed: 16988046]

Murase S, McKay RD. Matrix metalloproteinase-9 regulates survival of neurons in newborn hippocampus. J Biol Chem. 2012; 287:12184–12194. [PubMed: 22351756]

Murase S, Owens DF, McKay RD. In the newborn hippocampus, neurotrophin-dependent survival requires spontaneous activity and integrin signaling. J Neurosci. 2011; 31:7791–7800. [PubMed: 21613492]

Murthy VN, Schikorski T, Stevens CF, Zhu Y. Inactivity produces increases in neurotransmitter release and synapse size. Neuron. 2001; 32:673–682. [PubMed: 11719207]

Nagai M, Re DB, Nagata T, Chalazonitis A, Jessell TM, Wichterle H, Przedborski S. Astrocytes expressing ALS-linked mutated SOD1 release factors selectively toxic to motor neurons. Nat Neurosci. 2007; 10:615–622. [PubMed: 17435755]

Najjar S, Pearlman DM. Neuroinflammation and white matter pathology in schizophrenia: systematic review. Schizophrenia research. 2015; 161:102–112. [PubMed: 24948485]

Oppenheim RW. Cell death during development of the nervous system. Annu Rev Neurosci. 1991; 14:453–501. [PubMed: 2031577]

Pan L, North HA, Sahni V, Jeong SJ, McGuire TL, Berns EJ, Stupp SI, Kessler JA. beta1-Integrin and integrin linked kinase regulate astrocytic differentiation of neural stem cells. PloS one. 2014; 9:e104335. [PubMed: 25098415]

Peixoto RT, Kunz PA, Kwon H, Mabb AM, Sabatini BL, Philpot BD, Ehlers MD. Transsynaptic signaling by activity-dependent cleavage of neuroligin-1. Neuron. 2012; 76:396–409. [PubMed: 23083741]

Pfeiffer BE, Huber KM. Fragile X mental retardation protein induces synapse loss through acute postsynaptic translational regulation. J Neurosci. 2007; 27:3120–3130. [PubMed: 17376973]

Racine RJ. Modification of seizure activity by electrical stimulation. II. Motor seizure. Electroencephalography and clinical neurophysiology. 1972; 32:281–294. [PubMed: 4110397]

Rakhade SN, Jensen FE. Epileptogenesis in the immature brain: emerging mechanisms. Nature reviews Neurology. 2009; 5:380–391. [PubMed: 19578345]

Riedl SJ, Shi Y. Molecular mechanisms of caspase regulation during apoptosis. Nat Rev Mol Cell Biol. 2004; 5:897–907. [PubMed: 15520809]

Rohrbough J, Rushton E, Woodruff E 3rd, Fergestad T, Vigneswaran K, Broadie K. Presynaptic establishment of the synaptic cleft extracellular matrix is required for post-synaptic differentiation. Genes Dev. 2007; 21:2607–2628. [PubMed: 17901219]

Shen S, Lang B, Nakamoto C, Zhang F, Pu J, Kuan SL, Chatzi C, He S, Mackie I, Brandon NJ, Marquis KL, Day M, Hurko O, McCaig CD, Riedel G, St Clair D. Schizophrenia-related neural and behavioral phenotypes in transgenic mice expressing truncated Disc1. J Neurosci. 2008; 28:10893–10904. [PubMed: 18945897]

Sidhu H, Dansie LE, Hickmott PW, Ethell DW, Ethell IM. Genetic removal of matrix metalloproteinase 9 rescues the symptoms of fragile X syndrome in a mouse model. J Neurosci. 2014; 34:9867–9879. [PubMed: 25057190]

Smith AC, Kupchik YM, Scofield MD, Gipson CD, Wiggins A, Thomas CA, Kalivas PW. Synaptic plasticity mediating cocaine relapse requires matrix metalloproteinases. Nat Neurosci. 2014; 17:1655–1657. [PubMed: 25326689]

Soriano E, Cobas A, Fairen A. Asynchronism in the neurogenesis of GABAergic and non-GABAergic neurons in the mouse hippocampus. Brain Res. 1986; 395:88–92. [PubMed: 3022890]

Spolidoro M, Putignano E, Munafo C, Maffei L, Pizzorusso T. Inhibition of matrix metalloproteinases prevents the potentiation of nondeprived-eye responses after monocular deprivation in juvenile rats. Cereb Cortex. 2012; 22:725–734. [PubMed: 21685398]

Stawarski M, Rutkowska-Wlodarczyk I, Zeug A, Bijata M, Madej H, Kaczmarek L, Wlodarczyk J. Genetically encoded FRET-based biosensor for imaging MMP-9 activity. Biomaterials. 2014; 35:1402–1410. [PubMed: 24290700]

Szepesi Z, Hosy E, Ruszczycki B, Bijata M, Pyskaty M, Bikbaev A, Heine M, Choquet D, Kaczmarek L, Wlodarczyk J. Synaptically released matrix metalloproteinase activity in control of structural plasticity and the cell surface distribution of GluA1-AMPA receptors. PloS one. 2014; 9:e98274. [PubMed: 24853857]

Szklarczyk A, Lapinska J, Rylski M, McKay RD, Kaczmarek L. Matrix metalloproteinase-9 undergoes expression and activation during dendritic remodeling in adult hippocampus. J Neurosci. 2002; 22:920–930. [PubMed: 11826121]

Thiagarajan TC, Lindskog M, Tsien RW. Adaptation to synaptic inactivity in hippocampal neurons. Neuron. 2005; 47:725–737. [PubMed: 16129401]

Thyagarajan T, Totey S, Danton MJ, Kulkarni AB. Genetically altered mouse models: the good, the bad, and the ugly. Critical reviews in oral biology and medicine : an official publication of the American Association of Oral Biologists. 2003; 14:154–174.

Tsien RY. Very long-term memories may be stored in the pattern of holes in the perineuronal net. Proc Natl Acad Sci U S A. 2013; 110:12456–12461. [PubMed: 23832785]

Vargova L, Sykova E. Astrocytes and extracellular matrix in extrasynaptic volume transmission. Philosophical transactions of the Royal Society of London. Series B, Biological sciences. 2014:369.

Varley ZK, Pizzarelli R, Antonelli R, Stancheva SH, Kneussel M, Cherubini E, Zacchi P. Gephyrin regulates GABAergic and glutamatergic synaptic transmission in hippocampal cell cultures. J Biol Chem. 2011; 286:20942–20951. [PubMed: 21507951]

Vu TH, Shipley JM, Bergers G, Berger JE, Helms JA, Hanahan D, Shapiro SD, Senior RM, Werb Z. MMP-9/gelatinase B is a key regulator of growth plate angiogenesis and apoptosis of hypertrophic chondrocytes. Cell. 1998; 93:411–422. [PubMed: 9590175]

Wang XB, Bozdagi O, Nikitczuk JS, Zhai ZW, Zhou Q, Huntley GW. Extracellular proteolysis by matrix metalloproteinase-9 drives dendritic spine enlargement and long-term potentiation coordinately. Proc Natl Acad Sci U S A. 2008; 105:19520–19525. [PubMed: 19047646]

White AM, Williams PA, Ferraro DJ, Clark S, Kadam SD, Dudek FE, Staley KJ. Efficient unsupervised algorithms for the detection of seizures in continuous EEG recordings from rats after brain injury. J Neurosci Methods. 2006; 152:255–266. [PubMed: 16337006]

Wilczynski GM, Konopacki FA, Wilczek E, Lasiecka Z, Gorlewicz A, Michaluk P, Wawrzyniak M, Malinowska M, Okulski P, Kolodziej LR, Konopka W, Duniec K, Mioduszewska B, Nikolaev E, Walczak A, Owczarek D, Gorecki DC, Zuschratter W, Ottersen OP, Kaczmarek L. Important role of matrix metalloproteinase 9 in epileptogenesis. J Cell Biol. 2008; 180:1021–1035. [PubMed: 18332222]

Wlodarczyk J, Mukhina I, Kaczmarek L, Dityatev A. Extracellular matrix molecules, their receptors, and secreted proteases in synaptic plasticity. Developmental neurobiology. 2011; 71:1040–1053. [PubMed: 21793226]

Wong RO, Ghosh A. Activity-dependent regulation of dendritic growth and patterning. Nat Rev Neurosci. 2002; 3:803–812. [PubMed: 12360324]

Yeghiazaryan M, Rutkowska-Wlodarczyk I, Konopka A, Wilczynski GM, Melikyan A, Korkotian E, Kaczmarek L, Figiel I. DP-b99 modulates matrix metalloproteinase activity and neuronal plasticity. PloS one. 2014; 9:e99789. [PubMed: 24918931]

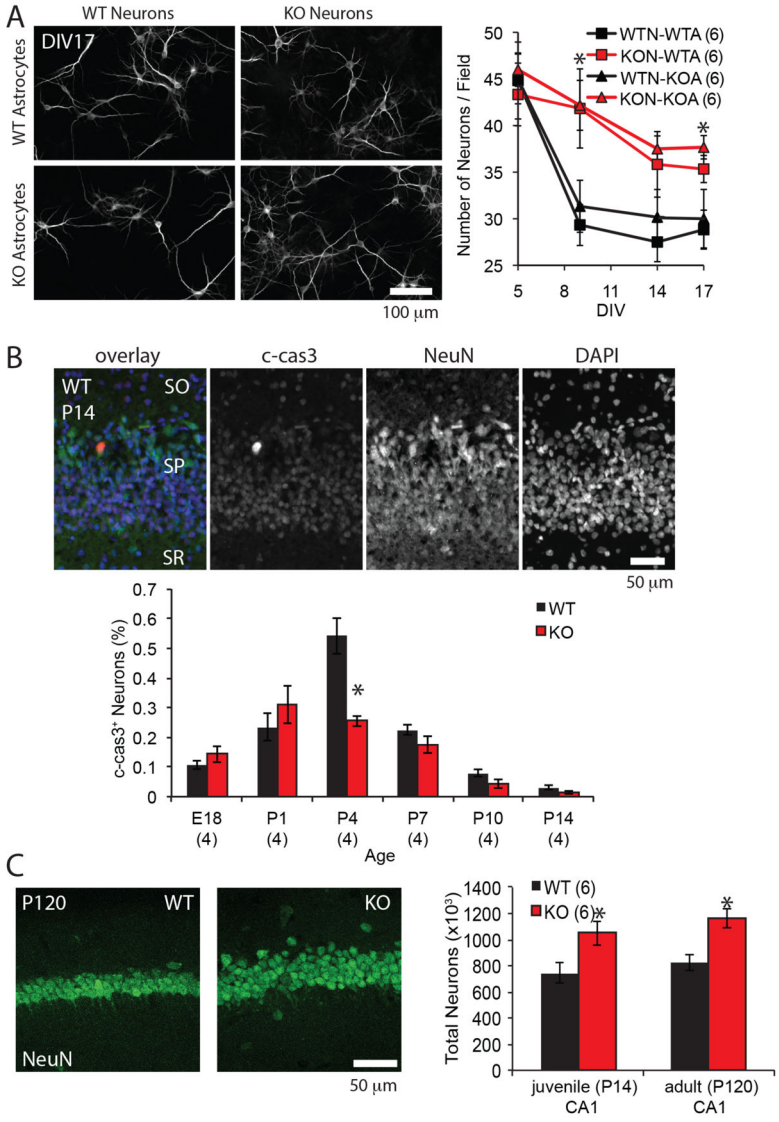

Figure 1. Suppression of neuronal death in MMP-9$^{-/-}$ hippocampus

(A) Hippocampal neurons from wild-type (WTN) and MMP-9$^{-/-}$ (KON) mice plated on astrocytes harvested from WT (WTA) or KO (KOA) mice. Left: Identification of neurons by immunostaining for the dendritic marker MAP2. Representative of each of four culture conditions at DIV17. Right: Change in neuronal density over development *in vitro* (n=6 cultures, Two-way repeated-measures ANOVA including all 4 culture conditions, $F_{(4,23)}$=2899; p<0.0001 *p<0.05 KON or KOA *vs.* WTN or WTA Tukey-Kramer post hoc test. (B) Top: Immunostaining of P14 wild type hippocampus for c-cas3 (red: apoptotic cells), NeuN (green: neurons) and DAPI (blue: nuclei). Bottom: Change in number of c-cas3^{+} neurons over development *in situ* (n=4 subjects, One-way repeated-measures ANOVA, $F_{(2,7)}$=11.5; p=0.015 *p<0.05 versus age-matched WT, Tukey-Kramer post hoc test). (C) Left: Immunostaining of P120 CA1 region of hippocampus for NeuN. Right: Stereological analysis of total number of CA1 stratum pyramidale (SP) neurons (n=6 subjects) at P14 and P120 *p<0.05; Student's T-test.

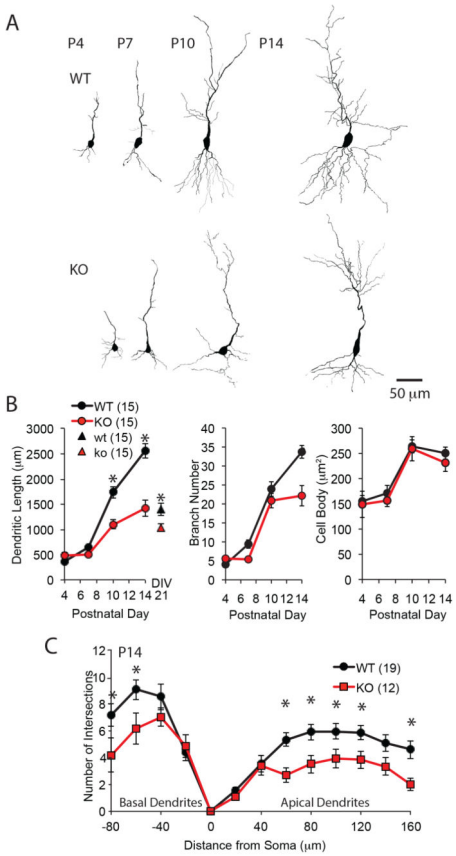

Figure 2. Constrained dendritic morphology of CA1 pyramidal neurons in MMP-9$^{-/-}$ mice

(A) Reconstruction of representative Golgi stained CA1 pyramidal neurons from WT (top) and MMP-9$^{-/-}$ (KO; bottom) mice at P4, P7, P10 and P14. (B) Quantification of total dendritic length, number of branches and size of cell bodies over development (n=15 neurons from 4 subjects each condition, One-way repeated-measures ANOVA, $F_{(2,29)}$=53.8; p<0.0001, 17.4; p<0.0001, and 1.05; p=0.314, respectively, *p<0.05, WT vs. KO, Tukey-Kramer post hoc test). Quantification of total dendritic length *in vitro* (n=15, neurons from 5 cultures for each group, *p=0.017, Student's T-test) shown for comparison triangles in B left. (C) Sholl analysis of number intersections of proximal dendrites. Distance from soma is plotted positively and negatively for apical and basal dendrites, respectively (n=19 neurons from 4 subjects for WT, 12 neurons from 4 subjects for KO. One-way repeated-measures ANOVA, $F_{(2,30)}$=11.3; p=0.002 and 4.58; p=0.041, respectively, *p<0.05, WT vs. KO, Tukey-Kramer post hoc test).

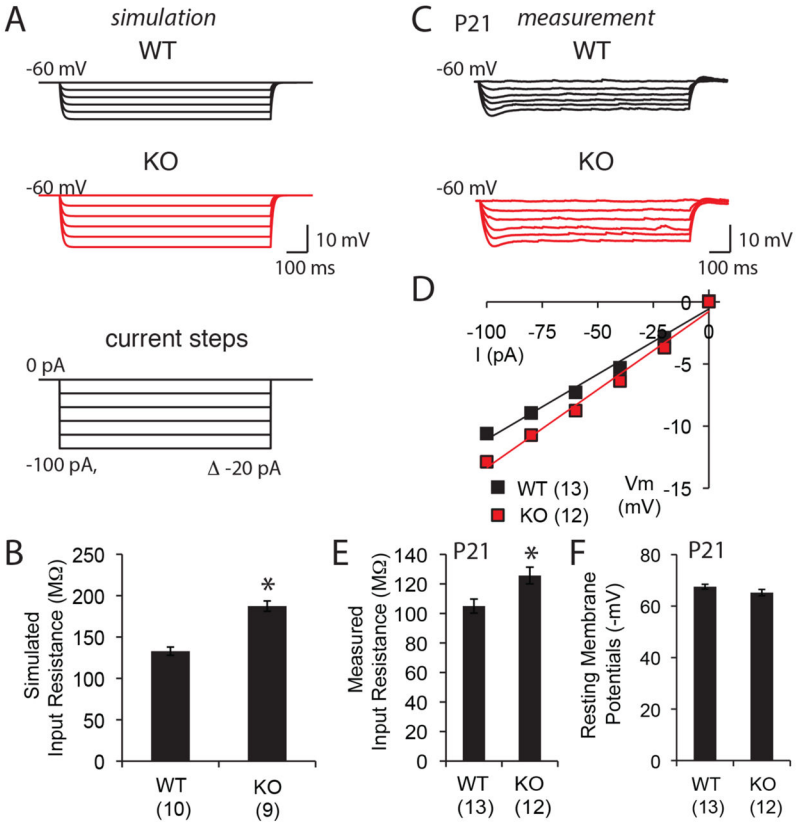

Figure 3. Higher input resistance in CA1 pyramidal neurons of MMP-9$^{-/-}$ mice

(A) Simulated steady-state voltage responses of WT and MMP-9$^{-/-}$ (KO) CA1 pyramidal neurons. Current injections (1000 ms somatic step) ranged from 0 pA to −100 pA in −20 pA increments. (B) Simulated values of input resistance (n=10 neurons from 4 subjects for WT, 9 neurons from 4 subjects for KO). (C) Real voltage responses of WT and KO CA1 pyramidal neurons. Injection of somatic step currents for 1000 ms ranging from 0 pA to −100 pA in −20 pA increments. (D) Current-voltage curve for WT and KO measured in real CA1 neurons. (E) and (F) Measurements of input resistance at −60 mV, and resting membrane potentials (n=13 neurons from 4 subjects for WT, 12 neurons from 4 subjects for KO). *p<0.05; Student's T-test.

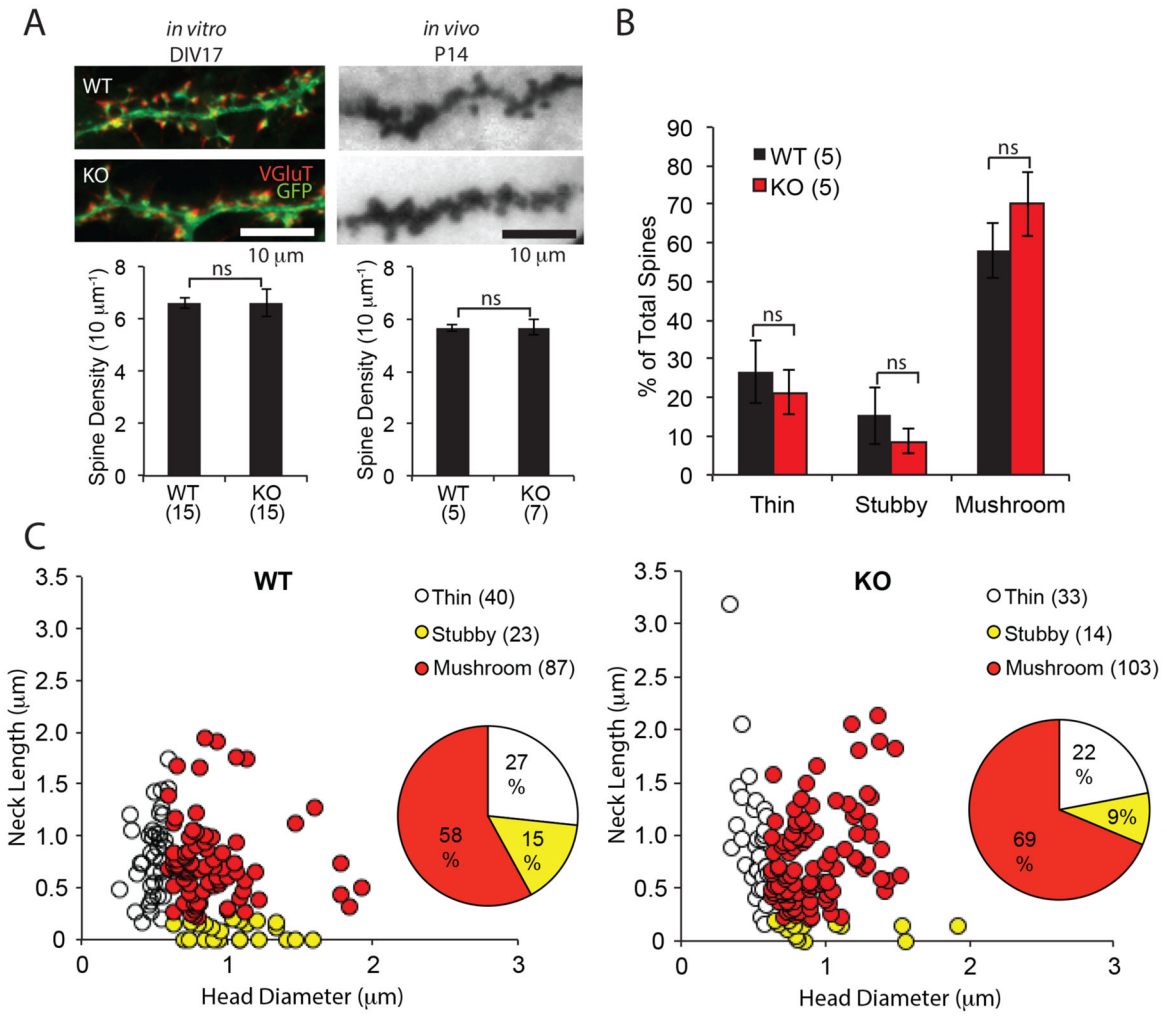

Figure 4. Normal dendritic spine density and morphology in MMP-9$^{-/-}$ hippocampal neurons

(A) Left top: Visualization of dendrites and spines via expression of GFP in cultured WT and MMP-9$^{-/-}$ (KO) hippocampal pyramidal neurons. Dendritic spines (green) colocalize with immunostaining for the pre-synaptic marker VGluT1 (red; DIV17). Left bottom: Mean dendritic spine density (n=15 neurons from 4 cultures, p=0.99; Student's T-test). Right top: Visualization of dendrites and spines *in situ via* Golgi staining of WT and MMP-9$^{-/-}$ (KO) CA1 hippocampal pyramidal neurons. Right bottom: Mean dendritic spine density (P14; n=5 neurons from 3 subjects for WT, 7 neurons from 3 subjects for KO, p=0.99, Student's T-test). (B) Proportion of different spine types: thin spines (spine head diameter<0.6 μm), stubby spines (neck length<0.2 μm), and mushroom spines (spine head diameter>0.6 mm and neck length>0.2 μm) in Golgi-stained WT and MMP-9$^{-/-}$ (KO) hippocampal CA1 pyramidal neurons at P14 (n=5 subjects each, 3 neurons were analyzed per subject, p=0.60, 0.43, 0.30, respectively; Student's T-test) (C) Distribution of head diameter and neck length of spines analyzed in B. Inset: contribution of each spine type to total (150 spines).

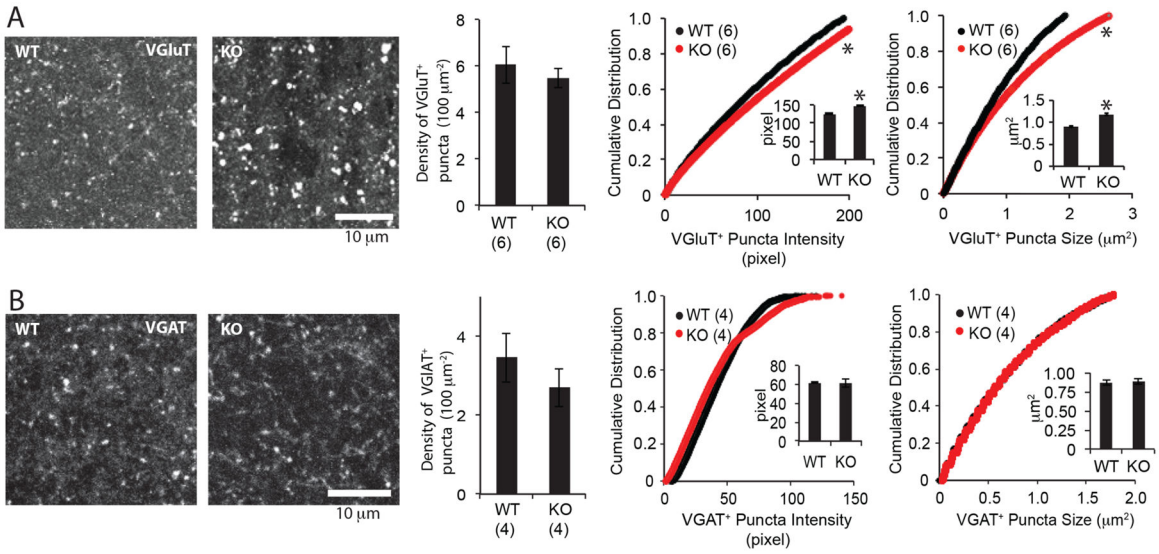

Figure 5. Distribution and size of presynaptic markers for excitatory and inhibitory synapses

(A) Left: representative immunostaining for glutamate transporter VGluT1. Middle: Mean ±SEM density of $VGluT^+$ puncta (n=6 hippocampi from 3 subjects, p=0.54; Student's T-test). Right: Cumulative distribution of $VGluT1^+$ puncta intensity and puncta size in CA1 SLM (n=6 hippocampi from 3 subjects). *p<0.05, K-S test (insets: Mean±SEM. *p<0.05; Student's T-test). (B) Left: representative immunostaining for GABA transporter VGAT. Middle: Mean±SEM density of $VGAT^+$ puncta (n=4 hippocampi from 4 subjects, p=0.85; Student's T-test). Right: Cumulative distribution of $VGAT^+$ puncta intensity and puncta size in CA1 SLM (n=4 hippocampi from 4 subjects). *p<0.05, K-S test (insets: Mean±SEM *p<0.05; Student's T-test).

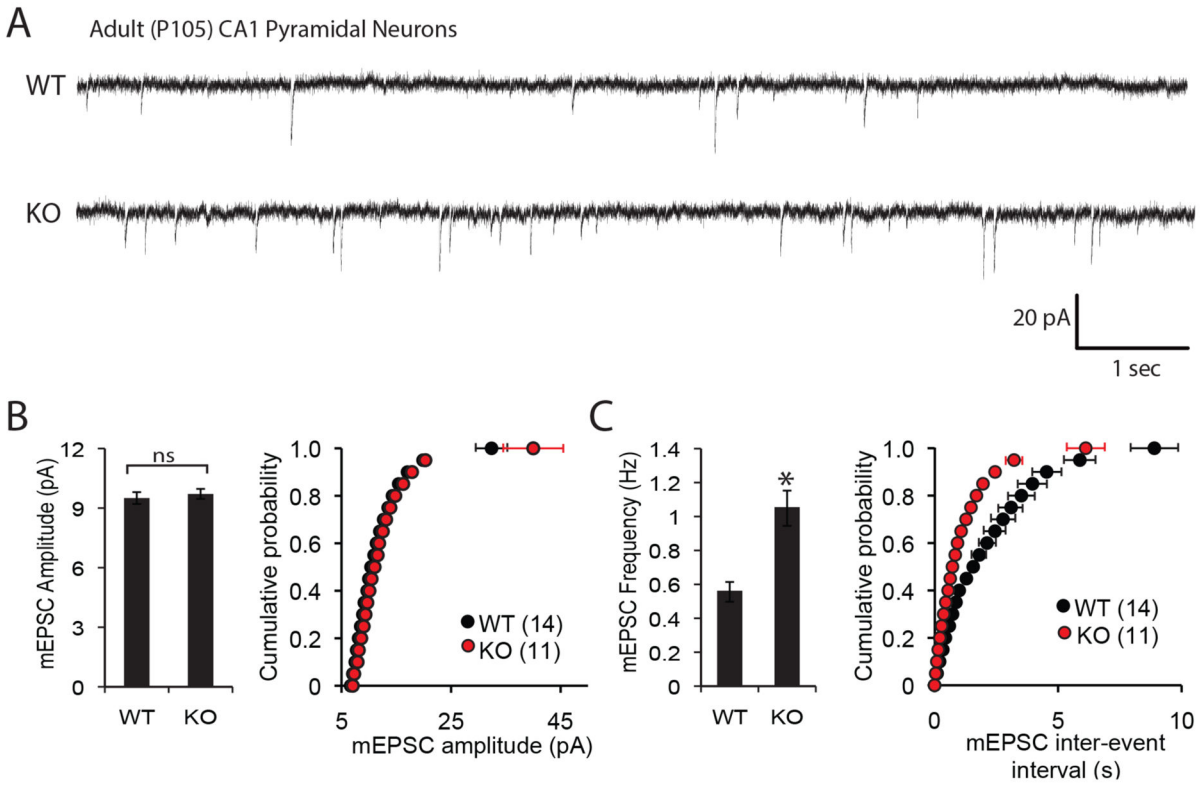

Figure 6. Change in excitatory synaptic transmission in MMP-9$^{-/-}$ mice

(A) Representative traces of mEPSCs from whole cell recordings of CA1 pyramidal neurons from WT and MMP-9$^{-/-}$ (KO) hippocampal slices. Average and cumulative probability distribution mEPSC amplitudes (B) and frequencies (C) of WT and KO CA1 pyramidal neurons (n=14 neurons from 4 subjects for WT, 11 neurons from 4 subjects for KO). *p<0.05; Student's T-test; p=0.119 for amplitude and 0.098 for frequency, K-S test.

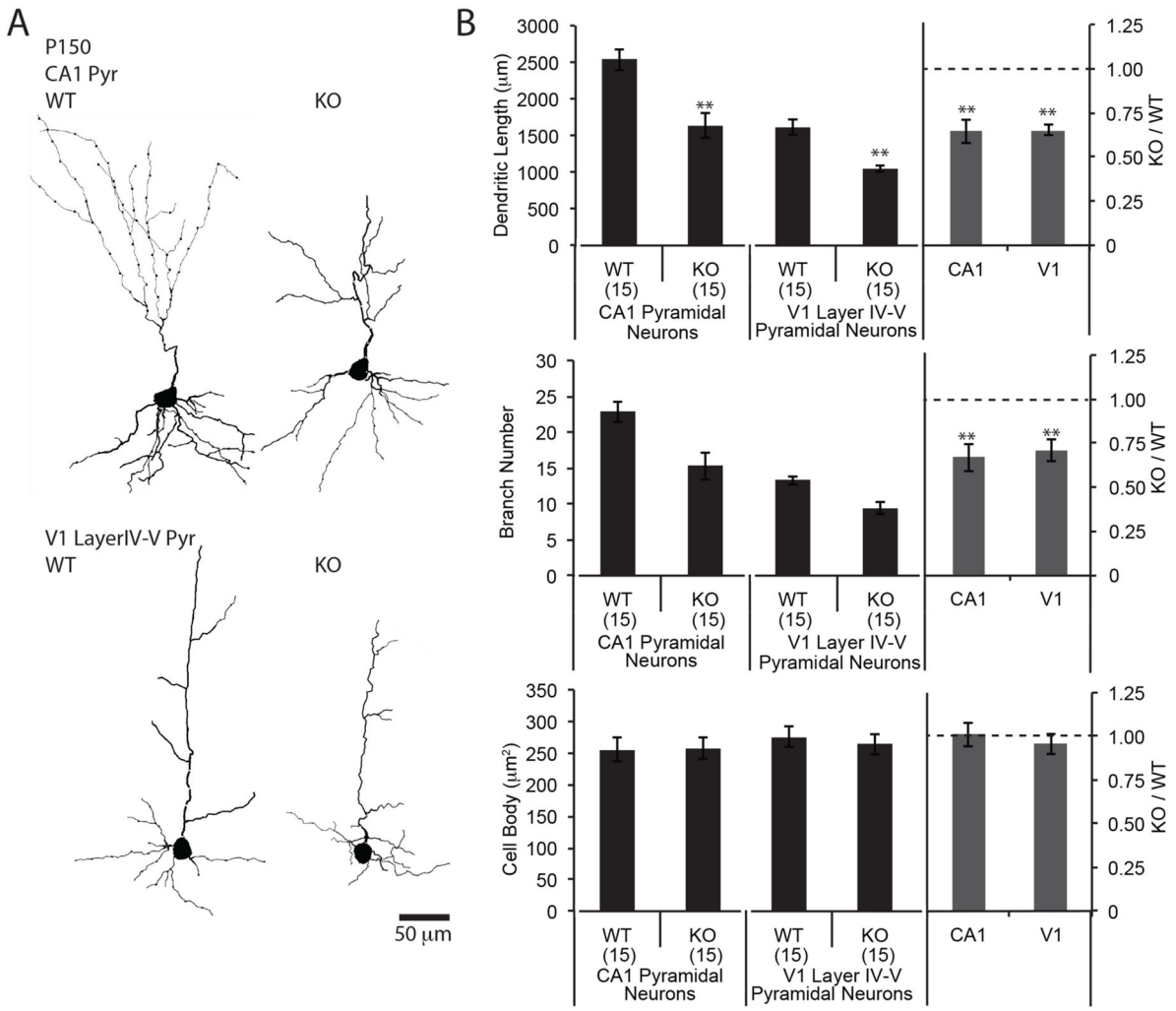

Figure 7. Constrained dendritic morphology in adult hippocampus and cortex in MMP-9$^{-/-}$ mice

(A) Reconstruction of representative Golgi stained neurons from CA1 region of hippocampus (top) and primary visual cortex (layer IV–V; bottom) from adult (P150) WT and MMP-9$^{-/-}$ (KO) mice. (B) Quantification of dendritic length, number of dendritic branches and size of cell bodies (n=15 neurons from 4 subjects, **p<0.001; Student's T-test,).

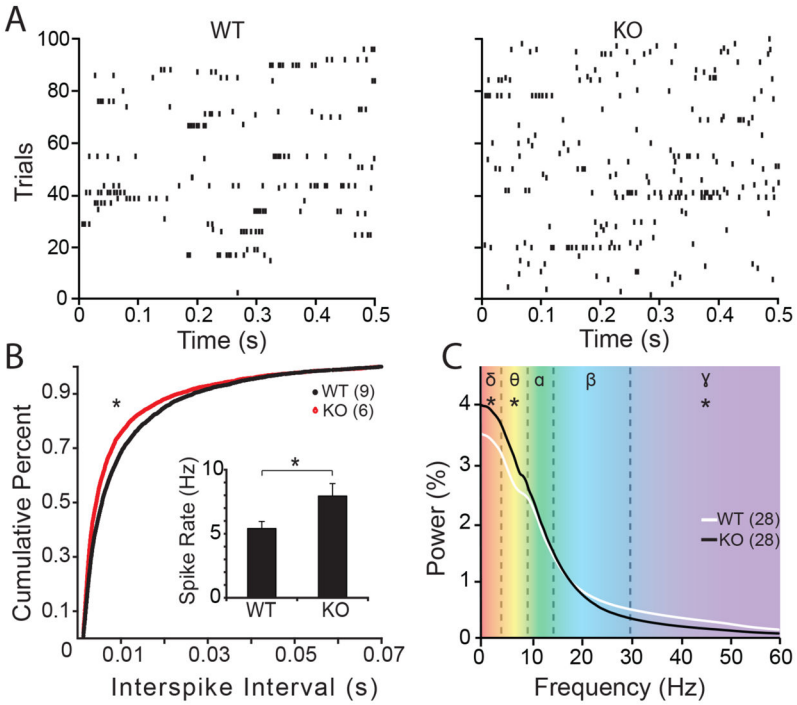

Figure 8. Enhanced spontaneous neuronal activity in MMP-9$^{-/-}$ cortex

(A) Raster plots of spontaneous output of single neurons (100 sweeps of 1 second observations) in WT and MMP-9$^{-/-}$ (KO) mouse. (B) Significant reduction in inter-spike intervals of spontaneous cortical activity in MMP-9$^{-/-}$ (KO) mice relative to WT (*p=0.047, K-S test). Inset: Significant increase in average rate of spontaneous activity in MMP-9$^{-/-}$ (KO) relative to WT (inset; n=9 subjects for WT, 6 subjects for KO; **p=0.02, Student's T-test). All single unit recordings were acquired from layer IV of primary visual cortex in awake subjects. (C) Power-spectrum density (PSD) analysis of spontaneous EcoG recordings for frequencies ranging from delta to gamma (n=28 recordings from 7 subjects for WT and KO. *p<0.05, Multivariate analysis of variance (MANOVA) for delta; f=7.014, p=0.011; theta; f=9.587, p=0.003; and gamma; f=14.003, p=0.000).

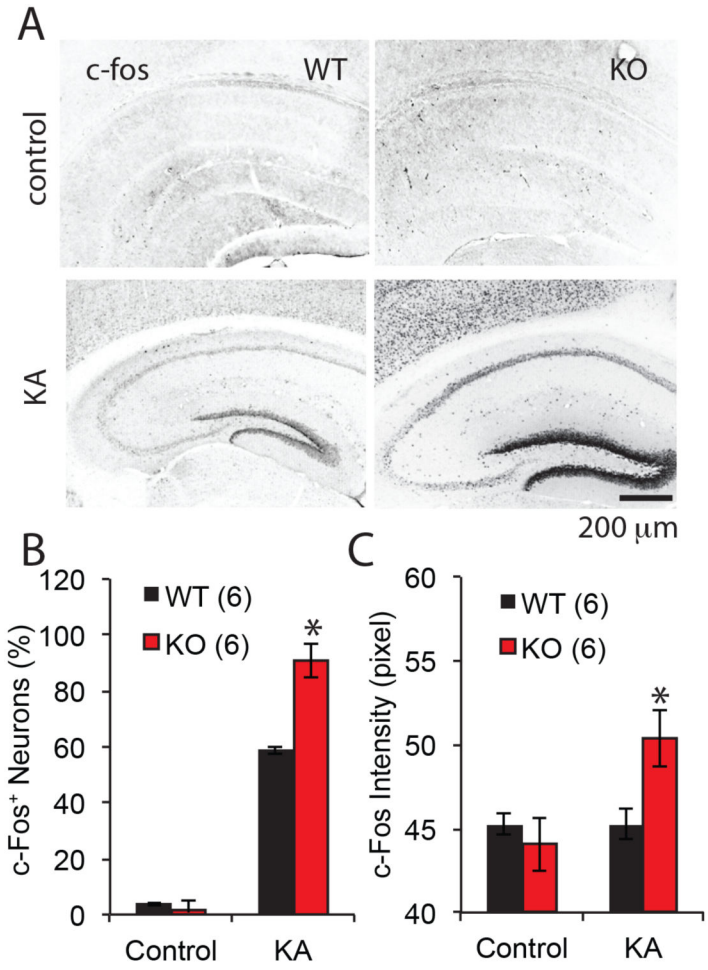

Figure 9. Increased c-fos expression following acute kainate challenge in MMP-9$^{-/-}$ mice

(A) Representative immunostaining for c-fos in P150 WT and MMP-9$^{-/-}$ (KO) mouse hippocampus, control and 2 hours after acute kainate challenge. (B) Quantification of the number of c-fos^{+} neurons in all hippocampal subfields. (C) Quantification of the intensity of c-fos staining. Control and 2 hr after acute kainate challenge (n=6 subjects). One-way ANOVA, $F_{(4,23)}$=137.5, p<0.001 for neuron number, $F_{(4,23)}$=4.698, p=0.012 for intensity. *p<0.05 WT-KA vs. KO-KA Tukey-Kramer post hoc.

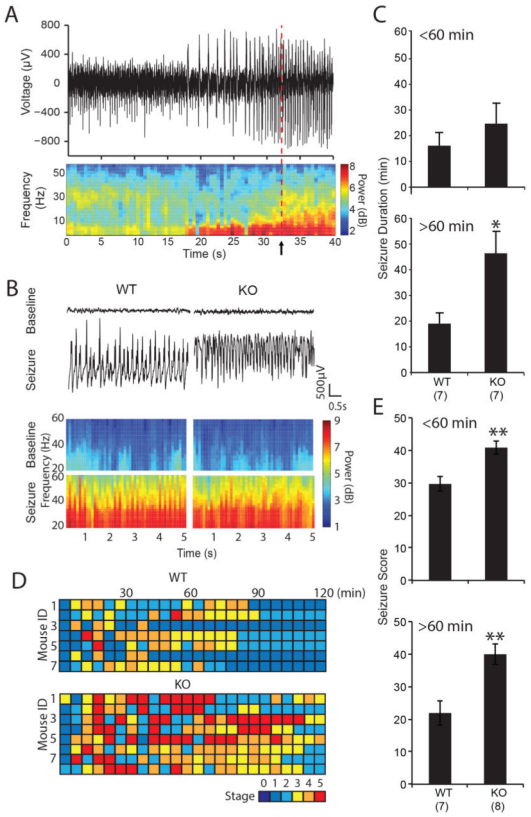

Figure 10. Increased duration of status epilepticus following acute kainate challenge in MMP-9$^{-/-}$ mice

(A) Representative example of ECoG recording (top) and power spectral analysis (bottom) of seizure initiation (arrow) identified by increase (2 standard deviations above average) in spiking frequency (top), power of theta frequency (4–8 Hz), and power of gamma frequency (30–60 Hz) (B) ECoG recording (top) and (power spectral analysis (bottom) from representative WT and MMP-9$^{-/-}$ (KO) mouse prior to kainate (baseline), and 30 minutes after kainate challenge (seizure). (C) Quantification of mean seizure duration for 0–60 min (top) and 61–120 min (bottom) following acute kainate challenge. *p<0.05; Student's T-test. (D) Behavioral analysis of response to acute kainate challenge. Racine scoring was performed every 5 min for 2hr, with observer blind to genotype. (E) Seizure scores of 0–60 min (top) and 61–120 min (bottom) following acute kainate challenge (n=7, 8 subjects for WT and KO, respectively, **p<0.001, Student's T-test).